

# A year-long evaluation of a wind-farm parameterisation in HARMONIE-AROME

Bart van Stratum<sup>1</sup>, Natalie E. Theeuwes<sup>2</sup>, Jan Barkmeijer<sup>2</sup>, Bert van Ulfst<sup>3</sup>, and Ine Wijnant<sup>2</sup>

<sup>1</sup>Wageningen University & Research

<sup>2</sup>Royal Netherlands Meteorological Institute (KNMI)

<sup>3</sup>Royal Dutch Meteorological Institute

November 23, 2022

## Abstract

The need to mitigate climate change will boost the demand for renewable energy and lead to more wind turbines both on- and onshore. In the near future, the effect these wind farms have on the atmosphere can no longer be neglected. In numerical weather prediction models wind-farm parameterisations (WFP) can be used to model the effect of wind farms on the atmosphere. There are different modelling approaches, but the parameterisation developed by Fitch et al. (2012) is most used in previous studies. It models the wind farm as a momentum sink and a source of power production and turbulent kinetic energy. In this paper, we have implemented the Fitch et al. (2012) WFP into HARMONIE-AROME, the numerical weather prediction model that is currently used by at least 11 national weather services in Europe. We used HARMONIE-AROME to make year-long simulations for 2016 with and without the WFP. The results were extensively evaluated using lidar, tower and flight measurements at several locations near wind farms. Including the WFP greatly reduces the model bias for wind speed near offshore wind farms. Wind farms not only affect wind, but also temperature and humidity, especially during stable atmospheric conditions: the enhanced mixing caused by the wind turbines reduces the stratification of temperature and humidity. Including the WFP in HARMONIE-AROME results in a more realistic representation of the atmosphere near wind farms and makes it a more future-proof model for weather forecasting.

# A year-long evaluation of a wind-farm parameterisation in HARMONIE-AROME

Bart van Stratum<sup>1,2</sup>, Natalie Theeuwes<sup>1\*</sup>, Jan Barkmeijer<sup>1</sup>, Bert van Uft<sup>1</sup>, Ine  
Wijnant<sup>1</sup>

<sup>1</sup>Royal Netherlands Meteorological Institute (KNMI), de Bilt, The Netherlands

<sup>2</sup>Department of Meteorology and Air Quality, Wageningen University, Wageningen, The Netherlands

## Key Points:

- In this study a wind-farm parameterisation is implemented in the numerical weather prediction model HARMONIE-AROME.
- A model evaluation of a full year reveals the wind-farm parameterisation greatly improves wind-speed forecasts close to offshore wind farms.
- The presence of wind farms in the model also alters temperature and humidity profiles due to the enhanced turbulent mixing by the turbines.

---

Corresponding author: Natalie Theeuwes, [natalie.theeuwes@knmi.nl](mailto:natalie.theeuwes@knmi.nl)

**Abstract**

The need to mitigate climate change will boost the demand for renewable energy and lead to more wind turbines both on- and onshore. In the near future, the effect these wind farms have on the atmosphere can no longer be neglected. In numerical weather prediction models wind-farm parameterisations (WFP) can be used to model the effect of wind farms on the atmosphere. There are different modelling approaches, but the parameterisation developed by Fitch et al. (2012) is most used in previous studies. It models the wind farm as a momentum sink and a source of power production and turbulent kinetic energy. In this paper, we have implemented the Fitch et al. (2012) WFP into HARMONIE-AROME, the numerical weather prediction model that is currently used by at least 11 national weather services in Europe. We used HARMONIE-AROME to make year-long simulations for 2016 with and without the WFP. The results were extensively evaluated using lidar, tower and flight measurements at several locations near wind farms. Including the WFP greatly reduces the model bias for wind speed near offshore wind farms. Wind farms not only affect wind, but also temperature and humidity, especially during stable atmospheric conditions: the enhanced mixing caused by the wind turbines reduces the stratification of temperature and humidity. Including the WFP in HARMONIE-AROME results in a more realistic representation of the atmosphere near wind farms and makes it a more future-proof model for weather forecasting.

**Plain Language Summary**

Wind power production is steadily increasing. Wind farms are growing both in number and size, while weather models evolve to higher resolutions. This means that the effect of wind farms can no longer be ignored by weather prediction models. Wind farms essentially decelerate the wind (blockage and wake effects) and increase turbulence, indirectly influencing temperature and humidity. In this study, we have included a widely used wind-farm parameterisation in the operational weather prediction model. The model is evaluated using various datasets, e.g. power production data, floating lidar measurements, and anemometer measurements from a tower. The inclusion of the wind-farm parameterisation improves the wind forecasts near wind farms, also improving the estimate in power production. In addition, we are able to model the effects of wind farms on the near-surface temperature and humidity.

## 45 1 Introduction

46 Offshore wind power production in the European Union (EU) and specifically the  
47 North-Sea region is steadily increasing: the Dutch offshore capacity is expected to grow  
48 from  $\pm 1$  GW in 2019 to  $\pm 11.5$  GW in 2030, as part of a total expected increase to  $\pm 70$   
49 GW in the entire EU (WindEurope, 2017). Wind turbines produce electric energy by  
50 extracting kinetic energy from the atmosphere, thereby decelerating (and agitating) the  
51 air. This typically results in a downstream decrease in wind speed and increase in tur-  
52 bulence (e.g. Baidya Roy & Traiteur, 2010; Fitch et al., 2012). As wind farms grow –  
53 both in size and number – the impact on weather and climate is expected to become more  
54 significant, requiring an adaptation of mesoscale models like HARMONIE-AROME (here-  
55 after: HARMONIE) to account for the influence of wind farms on the local and regional  
56 meteorological conditions.

57 There are several ways in which the effects of wind turbines on the atmosphere can  
58 be parameterised in mesoscale models (Fischereit et al., 2021). The implicit – imposing  
59 an additional roughness to implicitly model the effect of wind turbines on the atmospheric  
60 flow – or explicit, explicitly solving the momentum sink and enhanced turbulence pro-  
61 duction due to the presence of wind turbines. In the last two decades several explicit pa-  
62 rameterisations have been developed (e.g. Fitch et al., 2012; Abkar & Porté-Agel, 2015;  
63 Volker et al., 2015). The most commonly used and evaluated parameterisation is the Fitch  
64 et al. (2012) model implemented in the Weather Research and Forecasting (WRF) model  
65 (Skamarock et al., 2019).

66 In this study, we implemented the wind turbine parameterisation from Fitch et al.  
67 (2012) in HARMONIE. In the presence of wind turbines, this parameterisation adds an  
68 elevated drag term to the atmosphere, which locally decelerates the flow. The kinetic  
69 energy that is extracted from the atmosphere, but not converted into electric power, is  
70 used as a source term for turbulence kinetic energy (TKE).

71 HARMONIE with and without the newly-implemented wind-farm parameterisa-  
72 tion is evaluated using doppler lidar and tower measurements over the North Sea over  
73 a period of one full year (January up to and including December 2016), instead of eval-  
74 uating case studies as done in most evaluations of wind-farm parameterisations (e.g. Lee  
75 & Lundquist, 2017; Wu et al., 2022). During the full year, the parameterisation is eval-  
76 uated for all seasons with varying wind directions and atmospheric stabilities. In 2016,

77 measurements were available from two floating lidars in the Borssele wind farm zone (off  
 78 the Belgian coast), one ground-based lidar in the Westermost Rough wind farm (off the  
 79 east-coast of the UK), cup-anemometer measurements on the FINO1 tower near the Al-  
 80 pha Ventus wind farm (north of the Netherlands) and aircraft measurements (off the north-  
 81 west German coast). Since all these measurements are in or near existing wind farms,  
 82 they are ideal for evaluating the newly implemented wind-farm parameterisation. The  
 83 spatial impact of the wind farms on the wind fields is evaluated using dedicated flight  
 84 campaigns (Lampert, Bärfuss, et al., 2020). The consequence of the WFP on power pro-  
 85 duction is evaluated using Belgian transmission system operator (TSO) data. Moreover,  
 86 the year-long experiment allowed us to quantify the impact of the offshore wind farms  
 87 on the offshore and coastal meteorological conditions.

## 88 **2 HARMONIE-AROME**

89 The wind-farm parameterisation is implemented in HARMONIE-AROME (cycle  
 90 40h1), a non-hydrostatic model developed by the HIRLAM-C consortium, which is op-  
 91 erationally used in at least 11 countries (Bengtsson et al., 2017). The model uses a semi-  
 92 lagrangian scheme on an Eulerian grid. The turbulence scheme used was HARATU (de  
 93 Rooy et al., 2021; Lenderink & Holtslag, 2004), which uses a prognostic equation for the  
 94 turbulent kinetic energy (TKE), and shallow convection following de Rooy et al. (2021).  
 95 Surface Externalisée (SURFEX) version 7.3 was used as a land surface model (Masson  
 96 et al., 2013) with the land use classification from ECOCLIMAP II (Faroux et al., 2013).  
 97 More details about the model physics can be found in Bengtsson et al. (2017) or [www.hirlam.org](http://www.hirlam.org).

## 98 **3 Wind farm parameterisation**

99 The wind-farm parameterisation of (Fitch et al., 2012) imposes an elevated momen-  
 100 tum sink on the mean flow, where the drag (or thrust) of the individual turbine blades  
 101 is modelled as a constant (but wind speed dependent) drag force across the area swept  
 102 by the rotor blades. As the diameter of a wind turbine is about an order of magnitude  
 103 smaller than the horizontal grid spacing in HARMONIE (currently: 2.5 km), the model  
 104 accounts for the bulk influence of one or several wind turbines per grid point.

105 The wind turbine characteristics are defined by the geometry (hub-height  $z_{\text{hub}}$  and  
 106 turbine radius  $r$ ), the cut-in ( $V_{\text{in}}$ ) and cut-out ( $V_{\text{out}}$ ) wind speeds, and by the dimension-

107 less power ( $C_P$ ) and thrust ( $C_T$ ) coefficients. The latter two describe – as a function of  
 108 wind speed  $V_{\text{hub}}$  at hub height – the fraction of kinetic energy that is extracted from the  
 109 air ( $C_T$ ), and the fraction that is converted into electrical energy ( $C_P$ ). An example of  
 110 typical  $C_P$  and  $C_T$  curves is provided in Fig. 1.

111 Given the thrust coefficient  $C_T$ , the thrust force of a turbine (the force opposite  
 112 to the flow direction and drag force) is defined as:

$$113 \quad \vec{F}_{\text{thrust}} = -\frac{1}{2}\rho C_T |\vec{V}| \vec{V} A_T, [\text{N}] \quad (1)$$

114 where  $\rho$  is the air density ( $\text{kg m}^{-3}$ ),  $\vec{V} = (u, v)$  the horizontal wind vector ( $\text{m s}^{-1}$ ),  $|\vec{V}| =$   
 115  $\sqrt{u^2 + v^2}$ , and  $A_T$  is the rotor area ( $\text{m}^2$ ). The rate of loss of kinetic energy (KE) then  
 116 equals:

$$117 \quad \left. \frac{\partial \text{KE}}{\partial t} \right|_{\text{drag}} = -\frac{1}{2}\rho C_T |\vec{V}|^3 A_T. [\text{J s}^{-1}] \quad (2)$$

118 In practise the rotor of a turbine intersects multiple model levels, and Eq 2 (and all equa-  
 119 tions in the remainder of this chapter) are solved for each model level  $k$  individually, re-  
 120 placing the rotor area  $A_T$  with the area intersected by the  $k$ -th model level, and the wind  
 121 speed  $|\vec{V}|$ , and density  $\rho$  with values from the  $k$ -th model level, indicated where appro-  
 122 priate by a subscript  $k$ . As a result, the momentum sink (and TKE source) is elevated  
 123 and height dependent.

124 In general, the total change in KE of a single grid cell with a volume  $\Delta_k = (\Delta x \Delta y \Delta z_k)$   
 125  $\text{m}^3$  equals:

$$126 \quad \left. \frac{\partial \text{KE}_k}{\partial t} \right|_{\text{cell}} = \frac{\partial}{\partial t} \left( \frac{1}{2} \rho_k |\vec{V}_k|^2 \right) \Delta_k = \rho_k |\vec{V}_k| \frac{\partial |\vec{V}_k|}{\partial t} \Delta_k. [\text{J s}^{-1}] \quad (3)$$

127 Combining Eqs 2 and 3, i.e. setting:

$$128 \quad \left. \frac{\partial \text{KE}_k}{\partial t} \right|_{\text{cell}} = \left. \frac{\partial \text{KE}_k}{\partial t} \right|_{\text{drag}}, [\text{J s}^{-1}] \quad (4)$$

129 results, after re-arranging, in an expression for the change in velocity with time:

$$130 \quad \frac{\partial |\vec{V}_k|}{\partial t} = -\frac{1}{2} C_T |\vec{V}_k|^2 A_k \Delta_k^{-1}, [\text{m s}^{-2}] \quad (5)$$

131 or, in component form:

$$132 \quad \frac{\partial u_k}{\partial t} = -\frac{1}{2} C_T u_k |\vec{V}_k| A_k \Delta_k^{-1}, [\text{m s}^{-2}] \quad (6)$$

$$133 \quad \frac{\partial v_k}{\partial t} = -\frac{1}{2} C_T v_k |\vec{V}_k| A_k \Delta_k^{-1}. [\text{m s}^{-2}] \quad (7)$$

134 The vertical velocity component is assumed to be unaffected by the wind turbines, and  
 135 furthermore, drag by the wind turbine tower and nacelle is not included in the param-  
 136 eterisation. The energy that is extracted from the atmosphere, but not converted into  
 137 electrical energy, is assumed to be converted into turbulence kinetic energy (TKE, per  
 138 unit mass), i.e.  $C_{\text{TKE}} = C_T - C_P$ , resulting in:

$$139 \quad \frac{\partial \text{TKE}_k}{\partial t} = \frac{1}{2} C_{\text{TKE}} |\vec{V}_k|^3 A_k \Delta_k^{-1}. [\text{m}^2 \text{s}^{-2} \text{s}^{-1}] \quad (8)$$

140 Finally, as a diagnostic quantity, the model outputs the electrical power produced by the  
 141 wind turbines:

$$142 \quad P = \frac{1}{2} \rho C_P A_T |\vec{V}_{\text{hub}}|^3 [\text{W}] \quad (9)$$

143 For a typical offshore wind farm, multiple wind turbines can occupy a single horizontal  
 144 grid point. Instead of introducing a horizontal wind turbine density – like in (Fitch et  
 145 al., 2012) – Eqs 6 to 9 are repeated for each individual turbine, allowing different tur-  
 146 bine types in a single horizontal grid point. The total tendencies for the horizontal wind  
 147 components and TKE are adjusted after the turbulence scheme is called and fed back  
 148 to the model.

#### 149 **4 Experimental setup**

150 HARMONIE used a  $2000 \times 2000 \text{ km}^2$  domain with 65 vertical levels, 2.5 km hor-  
 151 izontal grid spacing, centred around  $51.96^\circ\text{N}$ ,  $4.9^\circ\text{E}$ . The ERA5 reanalysis (Hersbach et  
 152 al., 2020) is used for the lateral boundary conditions.

153 Two simulations were performed: (1) reference simulation without wind turbines,  
 154 REF, and (2) with the wind-farm parameterisation modelling all offshore wind turbines

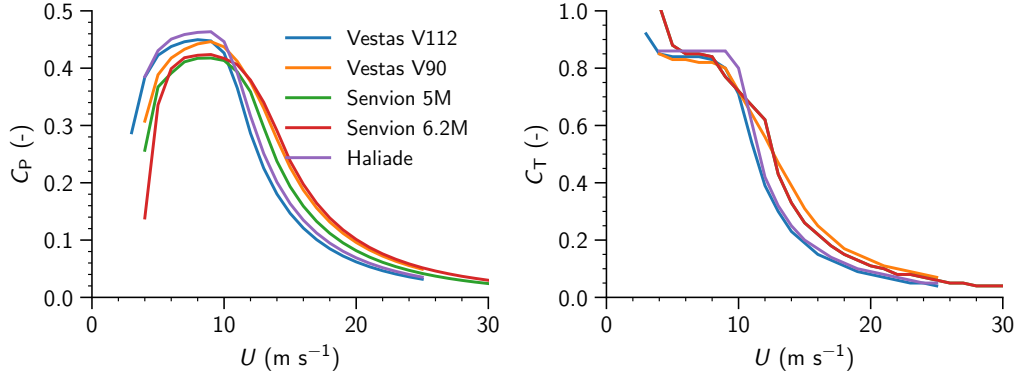


**Figure 1.** Power ( $C_P$ ) and thrust ( $C_T$ ) coefficients of the Belgian offshore wind turbines

155 present in the model domain in January 2016, WFP. The experiments are run from 01-  
 156 01-2016 00 UTC to 01-01-2017 00 UTC. This period was chosen because of the availabil-  
 157 ity of two floating lidars in the Borssele wind farm zone, directly north-east of the (Bel-  
 158 gian) Northwind wind farm (Fig. 2). In addition, for this period there are tower mea-  
 159 surements from the FINO1 platform, and lidar measurements from the Westermost Rough  
 160 wind farm and flights through wind farm wakes in the German Bight (WIPAFF; Lam-  
 161 pert, Bärfuss, et al., 2020).

162 The reference simulation was run for several years before the study period for the  
 163 Dutch Offshore Wind Atlas (DOWA) project (Wijnant et al., 2019) and therefore had  
 164 more than six years of spin-up. The WFP run was started ‘warm’ from the control ex-  
 165 periment and had ten days of additional spin-up time. Both reanalysis simulations used  
 166 3D-VAR data assimilation (Fischer et al., 2005; Gustafsson et al., 2018) with a three-  
 167 hour cycling time. In addition to conventional observations, Mode-S EHS aircraft mea-  
 168 surements (e.g. de Haan, 2011, 2016) and Scatterometer (ASCAT) (Marseille & Stof-  
 169 felen, 2017) were assimilated. In this study the 3-hour forecast is used as a proxy for the  
 170 analysis.

171 For the Belgian and Dutch wind farms, the exact (individual) turbine coordinates  
 172 are available, which could directly be used in the experiments. For the other offshore wind  
 173 farms in the computational domain (Fig. 2), the available information was limited to the  
 174 wind farm boundaries and the total number of turbines per wind farm. For these sites,  
 175 the turbine coordinates were first chosen randomly within the wind farm boundary, and  
 176 next distributed uniformly using an iterative repulsion method (Witkin & Heckbert, 2005).

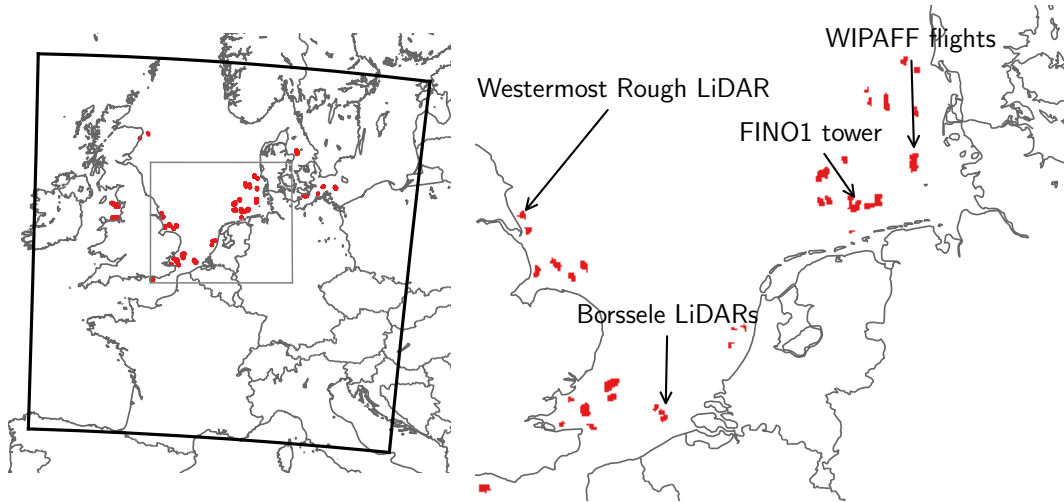


**Figure 2.** Overview of all (2.5×2.5 km) grid points with one or more wind turbines (red). Black arrows indicate the locations of measurements used for evaluation. In the left figure the black square indicates the model domain and the grey square the location of the right panel.

177 This random approach to determine the turbine coordinates can be justified by the fact  
 178 that within the turbine parameterisation, all turbines are mapped to the nearest 2.5 km  
 179 × 2.5 km grid point, making the exact turbine coordinates less important. The wind farm  
 180 boundaries were obtained from the *The European Marine Observation and Data Net-*  
 181 *work* (EMODnet; Martín Míguez et al., 2019).

182 The  $C_P$  and  $C_T$  curves were obtained from various sources, predominantly from  
 183 windPRO input database (Acker & Chime, 2011). For a small number of turbines, no  
 184  $C_P$  and  $C_T$  curves were publicly available, those turbines have been replaced with either  
 185 reference data from literature, or  $C_P$  and  $C_T$  curves from similar turbines. An overview  
 186 is provided in Appendix A.

## 187 5 Measurements

### 188 5.1 Borssele Wind Lidars

189 For the wind resource assessment of the four wind farms in the Borssele wind farm  
 190 zone (BWFZ), two short-range doppler lidars were deployed near the Belgian offshore  
 191 wind farms. Fugro executed a Metocean campaign and did measurements for a number

192 of periods between June 2015 and February 2017. ZephIR 300S lidars were mounted on  
 193 buoys with a bottom mooring weight at  $51.707^\circ$  N,  $3.035^\circ$  E (Fig. 3, lidar 1) and at  $51.646^\circ$   
 194 N,  $2.951^\circ$  E (Fig. 3, lidar 2). Lidar 1 (henceforth BWFZ1) measured for the longest pe-  
 195 riod and there were sixteen measurement periods between June 2015 and February 2017  
 196 (Fig. 4a). This lidar is located 10 km northeast of the nearest wind turbine. Lidar 2 (hence-  
 197 forth BWFZ2) only measured during five periods and only between February and July  
 198 2016 (Fig. 4b). This lidar is closer to the Belgian wind farm zones, at 2 km from the near-  
 199 est turbine (Fig. 3). At typical hub heights of about 90 m the uncertainty in floating li-  
 200 dar measurements for wind speeds between 4 and 15 m/s is between 3 and 4.5% (Duncan  
 201 et al., 2019)

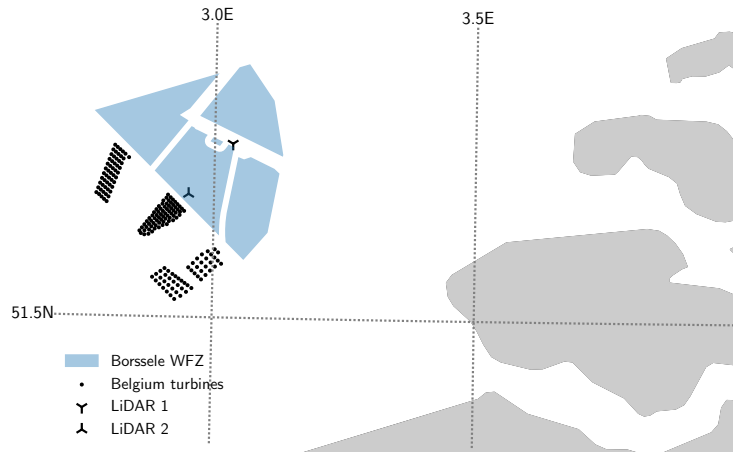


**Figure 3.** Setup of the Borssele wind lidars off the coast of Belgian and the Netherlands. The blue area are the planned wind farm zones, that started to be operational in 2020/2021.

## 202 5.2 FINO 1 Tower

203 The FINO 1 tower has been providing measurements since 2003 and is located in  
 204 the North Sea at  $54.015^\circ$  N,  $6.588^\circ$  E, 50 km north of the Wadden island Borkum (Fig.  
 205 2). The water depth at this location is 30 m and the tower reaches a height of 103.7 m  
 206 above Lowest Astronomical Tide (LAT). The first wind turbines were installed near FINO1  
 207 in November 2009 and the Alpha Ventus wind farm became fully operational in 2010.  
 208 This means that wind measurements for wind directions between  $15^\circ$  to  $165^\circ$  (easterly  
 209 winds) became disturbed by Alpha Ventus since November 2009. Borkum Riffgrund 1

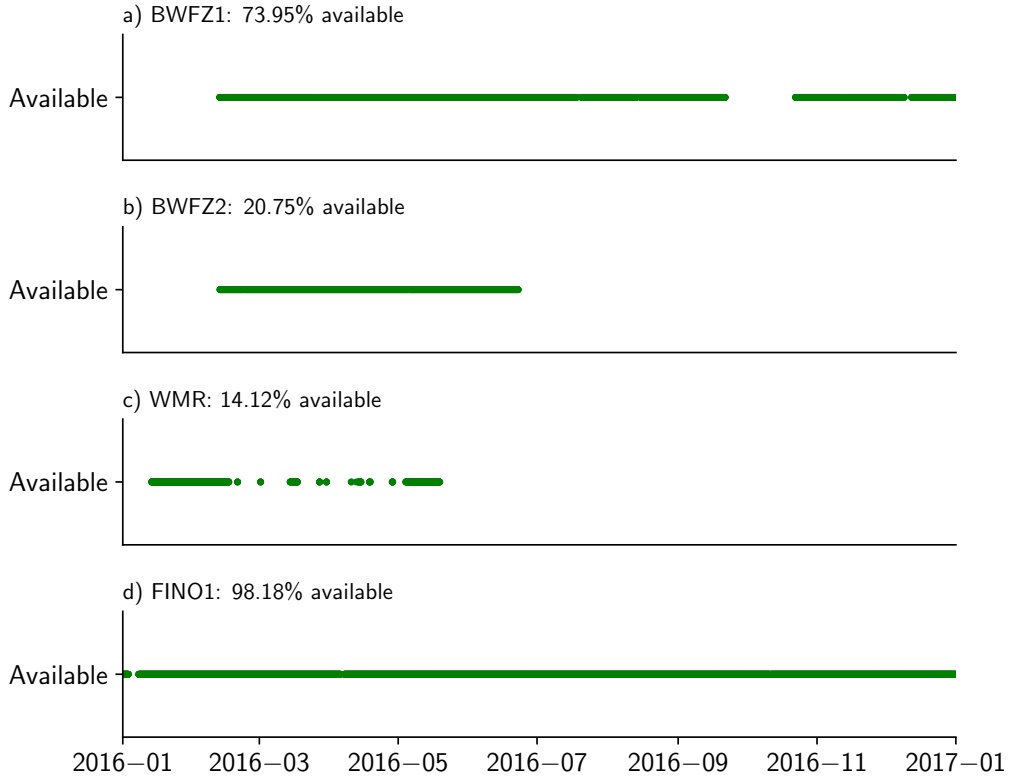


**Figure 4.** Availability of the measurements for the two lidars at the Borssele wind farm zone (a) BWFZ1 and (b) BWFZ2, (c) the Westermost Rough lidar (WMR) and (d) FINO 1.

210 to the south west has been fully operational since 2015, also disturbing the flow in 170°  
 211 to 300° directions.

212 Here, we use the cup anemometers to evaluate the model, since these measure at  
 213 frequent height intervals (i.e. 34.1, 41.6, 51.6, 61.6, 71.6, 81.6, 91.6, 101.6). The cup anemome-  
 214 ters are manufactured Vector Instruments Windspeed Ltd. type A100LK/PC3/WR with  
 215 an accuracy of 1 %. The cup anemometers (for measuring wind speed) are on booms on  
 216 the southeast side of the mast (towards 135–143°) and the wind vanes (for measuring  
 217 wind direction) on booms on the opposite side of the mast. The wind speed measure-  
 218 ments are corrected for wind mast effects using a measurement correction scheme called  
 219 the UAM-correction method Wind direction measurements are not corrected. (i.e. West-  
 220 erhellweg et al., 2010, 2012). Wind direction measurements are not corrected.

221 The FINO1 measurements are available for the whole of 2016 and only about 2.5  
 222 % of the data are missing (Fig. 4). Due to it’s long-term measurements the tower has

223 been previously used to evaluate atmospheric models over the North Sea (e.g. Muñoz-  
224 Esparza et al., 2012; Wagner et al., 2019).

### 225 **5.3 Westermost Rough Wind Lidar**

226 On top of the Westermost Rough wind farm substation (Fig. 2), Ørsted operates  
227 a Leosphere WindCube scanning doppler lidar, providing wind speed measurements be-  
228 tween 74 m to 324 m height. Westermost Rough wind farm is located off the coast of  
229 Yorkshire, UK. Unlike the Borssele lidars and FINO1 tower, this lidar is located in the  
230 centre of the wind farm ( $53.804^\circ$  N,  $0.132^\circ$  N), and is therefore always disturbed by the  
231 wind turbines. The Westermost Rough (WMR) lidar became operational in mid-January  
232 2016, but only has an overall availability of  $\sim 14\%$  (1.5 out of 12 months), which limits  
233 its usability.

### 234 **5.4 WIPAFF**

235 As part of the WInd PArk Far Field (WIPAFF) project (Platis et al., 2020), sev-  
236 eral measurements were taken around wind farms in the German Bight area (Fig. 2).  
237 In total 41 flights were carried out, of which 8 were in our current study period (6–10  
238 September 2016). The aircraft measurements were carried out using the research aircraft  
239 Dornier 128. The aircraft is equipped with sensors measuring temperature, humidity, all  
240 wind components, and pressure at 100 Hz. This large dataset of spatial data is very valu-  
241 able to evaluate mesoscale models with wind-farm parameterisations, and has been used  
242 previously to evaluate the Weather Research Forecasting model (WRF) (Platis et al.,  
243 2021). The measurements are described in detail by Lampert, Bärffuss, et al. (2020) and  
244 data are publicly available (Bärffuss et al., 2019).

245 For the purpose of this study we have only used one of the flights to evaluate the  
246 spatial representation of the wind farm wakes generated by HARMONIE. This flight took  
247 place on September 6 2016, between 12:13 and 15:20 downwind of Amrumbank West wind  
248 farm. During this day the average background wind speed was about  $7 \text{ m s}^{-1}$  from the  
249 south. Therefore the aircraft measurements were taken in a meandering pattern north  
250 of the wind farm at hub height (i.e. 90 m). Given the average speed of the plane was  
251  $54 \text{ m s}^{-1}$  and to compare with the model data at a grid spacing of 2.5 km, a 60-second  
252 rolling average over the sonic anemometer data is performed.

## 253 **5.5 Power production data**

254 Belgium's high-voltage TSO, Elia, publishes the generated power by their various  
255 energy sources, including offshore wind farm power production in 15-minute intervals.  
256 Since in 2016 Belgium only had three offshore wind farms (Fig. 2 & 3), we are able to  
257 use their power generation data to evaluate the HARMONIE-modelled generated power.  
258 The total capacity of these offshore wind farms was 712.2 MW.

## 259 **6 Evaluation**

### 260 **6.1 Offshore lidar and tower measurements**

261 During the chosen period, all lidars had periods with missing data, as summarised  
262 in Fig. 4. For all statistical analyses in this section we use collocated data, i.e. missing  
263 data is removed (or masked) in the model dataset as well. In addition, there is no con-  
264 ditional sampling based on (e.g.) wind direction; all available measurements are always  
265 included in the statistics.

#### 266 **6.1.1 Borssele Wind Farm Zone (BWFZ) lidars**

267 As shown in Fig. 3, both lidars were positioned north-east of the Belgian North-  
268 wind wind farm. With prevailing winds from the south-west, these lidar measurements  
269 are typically disturbed by the Belgian wind farms, making them ideal for assessing the  
270 impact of the wind turbines on the wind field, and the ability of the wind farm parametri-  
271 sation to reproduce the disturbed wind field due to the wake effect of the wind farm.

272 Figure 5 shows the time averaged vertical wind speed profiles from the reference  
273 run (REF), the experiment with the wind-farm parameterisation (WFP), and the Bors-  
274 sele lidars. These are averaged profiles over the entire measurement period for both li-  
275 dars and represent all different wind directions. However, over the duration of the mea-  
276 surement period of BWFZ1, the wind direction was southwesterly ( $180\text{--}270^\circ$ ) 42% of the  
277 time.

278 For both sites the reference simulation (without wind park parameterisation) over-  
279 estimates the wind speed, which is most pronounced for lidar location number two, which  
280 is closest to the Belgian wind farms at 2 km distance from the nearest turbine. Enabling

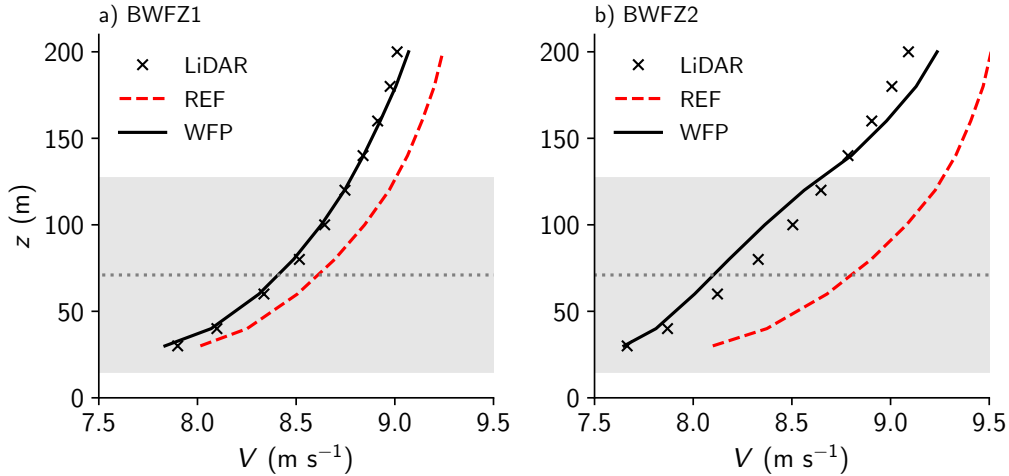


**Figure 5.** Vertical profiles of wind speed, from the reference run (REF) and experiment with wind-farm parameterisation (WFP), compared to the Borssele (a) BWFZ lidar 1, 10 km from the nearest wind farm and (b) BWFZ lidar 2, 2 km from the nearest wind farm. The grey dotted line indicates the mean hub height of the nearest wind farm and the grey shaded areas the area the diameter of the rotor.

281 the wind-farm parameterisation clearly improves the experiments; for BWFZ2, the mean  
 282 profile from HARMONIE matches very well with the measurements.

### 283 6.1.2 FINO1 tower

284 The FINO1 tower is situated directly west of the Alpha Ventus wind farm, and north-  
 285 east of the Borkum Riffgrund wind farm (Fig. 2). Fig. 6a shows the time averaged ver-  
 286 tical wind speed profiles, compared to the corrected FINO1 measurements. In line with  
 287 the results from the Borssele area, the reference simulation overestimates the wind speed  
 288 with  $\sim 0.7\text{--}0.9\text{ m s}^{-1}$ . With the wind-farm parameterisation included, the absolute bias  
 289 is decreased, but with a slight negative bias at the highest few measurement points,  $\sim 0.1\text{--}$   
 290  $0.2\text{ m s}^{-1}$ . This underestimation seems to be partially caused by the mapping of wind  
 291 turbines to the nearest HARMONIE grid point. In reality the FINO1 tower is west (and  
 292 with the dominating wind direction: upstream) of the Alpha Ventus wind farm, but in  
 293 HARMONIE the grid point nearest to FINO1 also houses some of the Alpha Ventus wind  
 294 turbines, as shown in Fig. 6b. This means that the grid point used for the analysis, di-  
 295 rectly experiences drag from some of the Alpha Ventus turbines, resulting in a reduced  
 296 wind speed. However, including the wind-farm parameterisation clearly improves the wind

297 profile at the tower location due to the many wind farms in the surroundings. This is  
 298 also the location where the largest impact is expected.

299 **6.1.3 Westermost Rough lidar**

300 As shown in Fig. 4, the data availability is limited to  $\sim 14\%$  of the January to May  
 301 period, and even less at the three highest measurement heights. Therefore, the analy-  
 302 sis here is limited to the lowest 214 m.

303 Fig. 7 shows the time averaged vertical profiles of the lidar measurements and HAR-  
 304 MONIE experiments. As with the FINO1 and Borssele locations, the reference run over-  
 305 estimates the wind speed. The experiment with wind turbines (WFP) is very close to  
 306 the averaged lidar observations, especially near hub height. Above the rotor tips the gra-  
 307 dient at which the wind speed increases is underestimated in the model. This results in  
 308 a bias at 214 m of  $0.2 \text{ m s}^{-1}$  for the REF experiment and  $0.3 \text{ m s}^{-1}$  for the WFP ex-  
 309 periment. Since the REF experiment also underestimates the wind speed above the ro-  
 310 tor tip, this bias could be caused by an underestimation of the background wind speed  
 311 or a measured acceleration of the wind above the rotor tip not captured by HARMONIE  
 312 with the WFP.

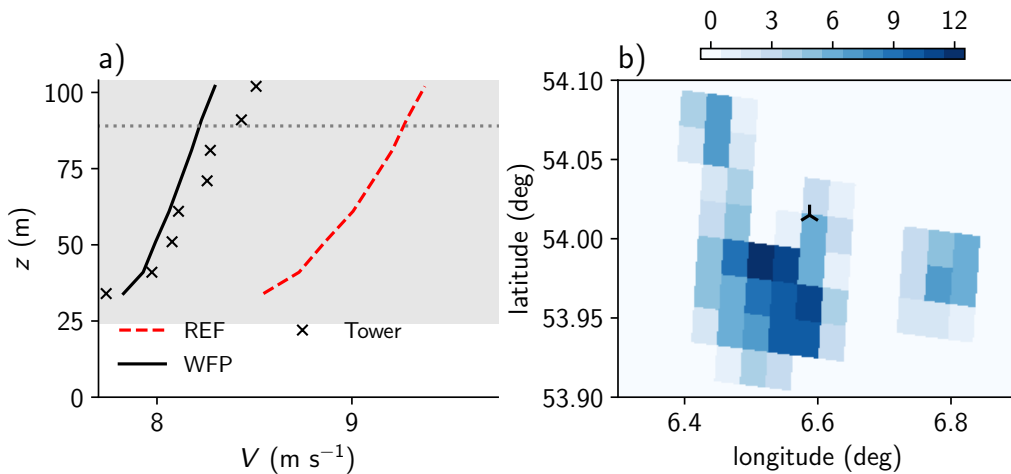


**Figure 6.** (a) Vertical profiles of wind speed, from the reference run without wind-farm parameterisation (REF) and experiment with wind-farm parameterisation (WFP), compared to the FINO1 tower. (b) The number of turbines in the HARMONIE grid cells surrounding FINO1

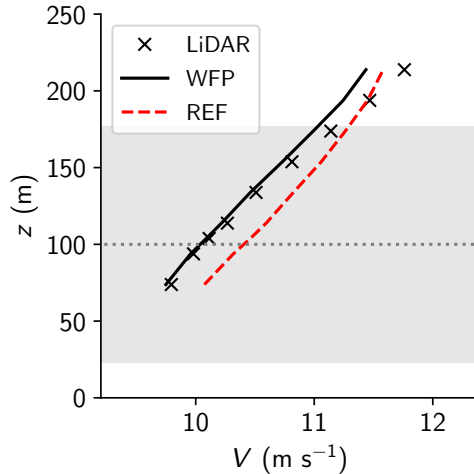


**Figure 7.** Vertical profiles of wind speed, from the reference run without wind-farm parameterisation (REF) and experiment with wind-farm parameterisation (WFP), compared to the Westermost rough lidar.

313

## 6.2 Airbourne measurements

314

315

316

317

318

319

320

321

322

323

324

325

For the evaluation of HARMONIE with the wind-farm parameterisation the lidar and tower measurements show significant improvements at single locations. However, in order to evaluate the spatial scale of the modelled wakes airbourne measurements are used. The WIPAFF measurement flights are intended to observe the spatial extent of the wind-farm wakes. As mentioned in sect. 5.4, we only use the airbourne measurements carried out during 6 September 2016, with a near-neutral – slightly stable surface layer and an average wind speed of  $7 \text{ m s}^{-1}$ . In those cases we expect to see a large wake from the wind farm, but not as strong as in very stable conditions (e.g. Zhan et al., 2020). Fig. 8 compares the flight measurements with the HARMONIE simulations following the same model track. For each measurement point the nearest model point in time and space was extracted for both REF and WFP simulations. The model output was interpolated between the nearest two model levels to 90 m, the flying altitude.

326

327

328

329

330

Close to the wind farm the wind farm wake is captured very well by the WFP (Fig. 8a). Here, at  $\sim 4 \text{ km}$  distance the velocity deficit is about  $2 \text{ m s}^{-1}$  and the width of the wind farm is about  $15 \text{ km}$ . During this time the background wind speed decreases left to right of the wind farm (negative to positive  $x - \overline{x_{\text{turbines}}}$ ), however this is underestimated by the model leading to a bias of  $1.0 \text{ m s}^{-1}$  in the WFP run. An 1.5 hours later

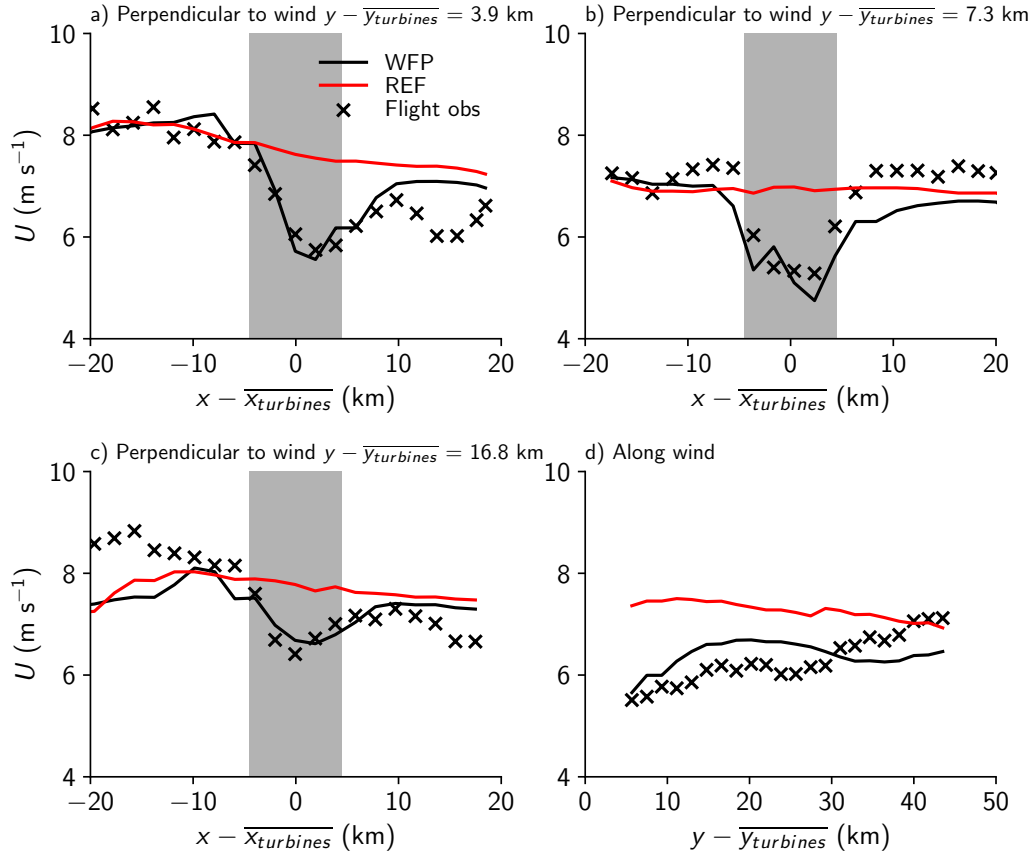


**Figure 8.** Cross sections through the wind farm wake of Amrumbank West in the German Bight on 6 September 2016, 12:13 – 15:20 UTC. Cross sections are perpendicular to the wind direction at (a) 3.9 km (b) 7.3 km, and (c) 16.8 km distance from the turbines, and (d) a cross section along the wind from the centre of the turbines directly downstream. Crosses indicate 60 s rolling average wind speeds at 30 s intervals from the aircraft measurements and lines indicate the interpolated modelled wind speed along the same flight path (red) reference run and (black) simulation with WFP. The grey are indicate the location of the wind farm.

331 ( $\sim 14:30$ ) a cross section was taken at about 7.3 km downwind of the wind farm (Fig. 8b).  
 332 Here, the HARMONIE WFP run is able to capture the wind speed in the wake of the  
 333 turbines very well, but now underestimates the wind speed east of the turbines (posi-  
 334 tive  $x - \overline{x_{\text{turbines}}}$ ) by about  $0.7 \text{ m s}^{-1}$ . About 10 km downwind of the previous cross  
 335 section (Fig. 8c), the velocity deficit in the wind-farm wake has been reduced to  $\sim 1 \text{ m}$   
 336  $\text{s}^{-1}$ , captured well by in the WFP run. As expected, the REF run is unable to model  
 337 the velocity deficit caused by the wind farm.

338 The part of the flight along the wind direction captures the recovery of the wake  
 339 (Fig. 8d). About 4 km away from the wind farm the wind speed is  $5.4 \text{ m s}^{-1}$ , at 30 km  
 340 away the wind speed has only increased by  $0.7 \text{ m s}^{-1}$  to  $6.1 \text{ m s}^{-1}$ . Over the same dis-  
 341 tance the model shows a similar reduction in the velocity deficit,  $0.8 \text{ m s}^{-1}$ . After 30 km  
 342 the observations show the wake to dissipate quickly, while in HARMONIE there remains  
 343 a difference between the REF and WFP runs of about  $< 0.5 \text{ m s}^{-1}$  for at least 70 km down-  
 344 wind of the wind farm. The Fitch et al. (2012) parameterisation is known to produce  
 345 long wakes (e.g. Shepherd et al., 2020). However, a more systematic evaluation of the  
 346 size and shape of wakes using Fitch et al. (2012) is needed, with more research aircraft  
 347 data, scanning doppler lidars (e.g. Rhodes & Lundquist, 2013; Banta et al., 2015), or  
 348 satellite measurements such as SAR (e.g. Christiansen & Hasager, 2005).

### 349 **6.3 Power production**

350 When evaluating HARMONIE with the wind-farm parameterisation, power produc-  
 351 tion is a crucial quantity. Power production scales with the velocity cubed (eq. 9),  
 352 making it sensitive to biases in wind speed. For all of 2016, Elia provides power produc-  
 353 tion data for the Belgian offshore wind farms. This is the total power production of all  
 354 the offshore wind farms. In 2016 these farms had a total capacity of 712.2 MW (Fig. 3).

355 Figure 9 shows the comparison between the observed power production and power  
 356 production obtained from the HARMONIE experiments, both from the reference exper-  
 357 iment and experiment with the wind turbine parameterisation (WFP). The bottom pan-  
 358 els indicate the absolute and relative differences, averaged over 50 MW bins. The rel-  
 359 ative bias from the first (0-50 MW) bin should be treated with caution, as conditions  
 360 where the observed power production equals zero result in an infinitely large relative bias.

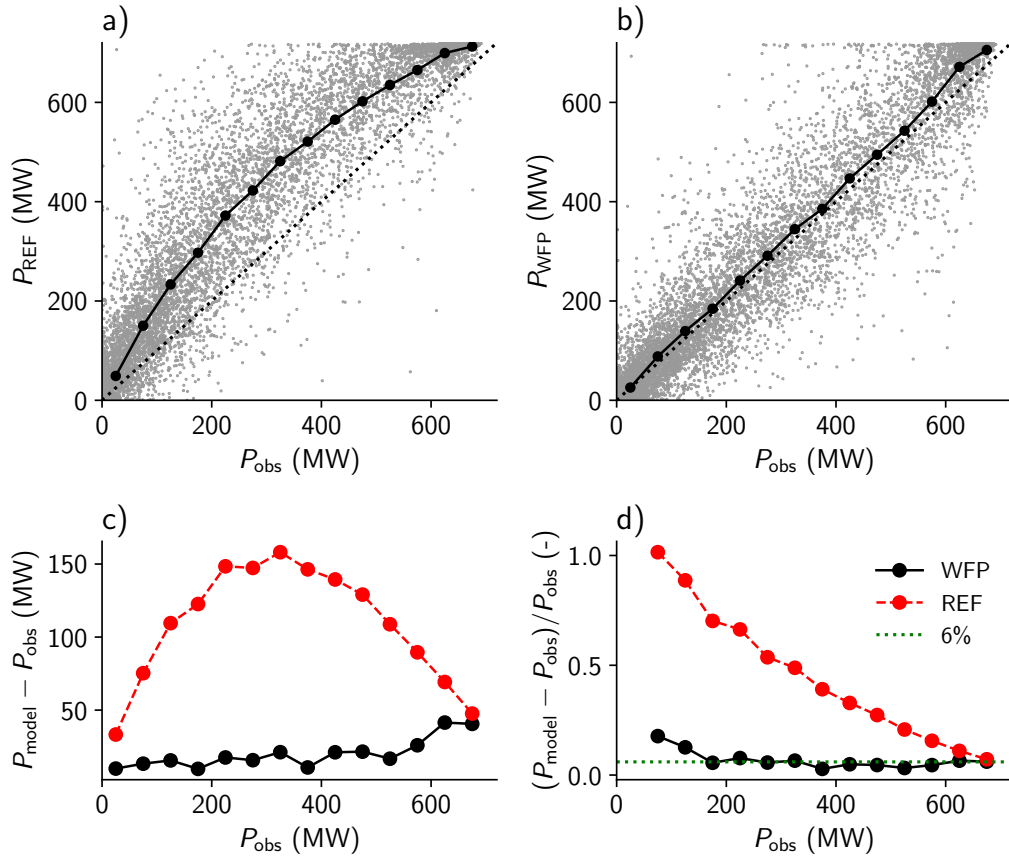


**Figure 9.** Power production calculated from the (a) reference reanalysis (REF) and (b) experiment with wind-farm parameterisation (WFP), compared to the Elia measurements. The solid black line with markers (top row) indicates the mean of the model data calculated over 50 MW bins. The bottom row shows the absolute (c) and relative (d) error of both model experiments.

361 The power production calculated offline (eq. 9) from the reference experiment clearly  
 362 overestimates the production, with absolute biases as large as 150 MW, and for low wind  
 363 speeds (low power production) relative biases as large as 100%. The reference simula-  
 364 tion clearly does not include the power production losses attributed to the velocity deficit  
 365 created by the wind turbines. Including the wind turbine parameterisation clearly im-  
 366 proves the power production calculated, reducing the absolute bias to a maximum of 50  
 367 MW at high wind speeds, and the relative bias to  $\sim 6\%$ . There are a few possible causes  
 368 for this constant relative bias – e.g. efficiency losses in the turbines or power cables, the  
 369 use of (manufacturers) turbine specifications which are too optimistic, inaccuracies in  
 370 the turbine parameterisation, or single turbines that are not operational, or not func-  
 371 tioning optimally. If the aim is to deliver power production forecasts to users, some post  
 372 processing will be necessary to eliminate these inaccuracies.

#### 373 **6.4 Impact wind farms on local meteorological conditions**

374 As seen in the previous sections, wind turbines have an impact on the (local) wind  
 375 conditions. In addition, wind turbines generate TKE, which enhances vertical mixing,  
 376 potentially influencing other quantities like temperature, humidity, or clouds. Here, we  
 377 briefly examine the impact of two Dutch offshore wind farms on the local meteorolog-  
 378 ical conditions. In the absence of suitable measurements, the results are limited to com-  
 379 paring the reference simulations with the experiment including wind turbines.

380 Fig. 10 shows the differences in wind speed ( $V$ ), potential temperature ( $\theta$ ), and spe-  
 381 cific humidity ( $q$ ) between the experiments with and without wind turbines for two time  
 382 periods. During the period March – June the sea surface temperature is colder on av-  
 383 erage compared to the atmospheric temperature and more stable cases are expected. Dur-  
 384 ing September – December the sea surface temperature is generally warmer than the at-  
 385 mosphere above, leading to more unstable cases. For each wind farm, the statistics were  
 386 averaged over the HARMONIE grid points which have one or more turbines, and aver-  
 387 aged in time.

388 For wind speed, the elevated drag is clearly visible, with a maximum decrease of  
 389  $1.6 \text{ m s}^{-1}$  near hub height, but a near-surface decrease of  $0.3 - 0.0 \text{ m s}^{-1}$ . The relatively  
 390 small wind farm Princes Amalia (120 MW,  $-0.6 \text{ m s}^{-1}$  during spring and  $-0.5 \text{ m s}^{-1}$  in  
 391 autumn) has a smaller impact on the wind speed compared to the larger Gemini (600

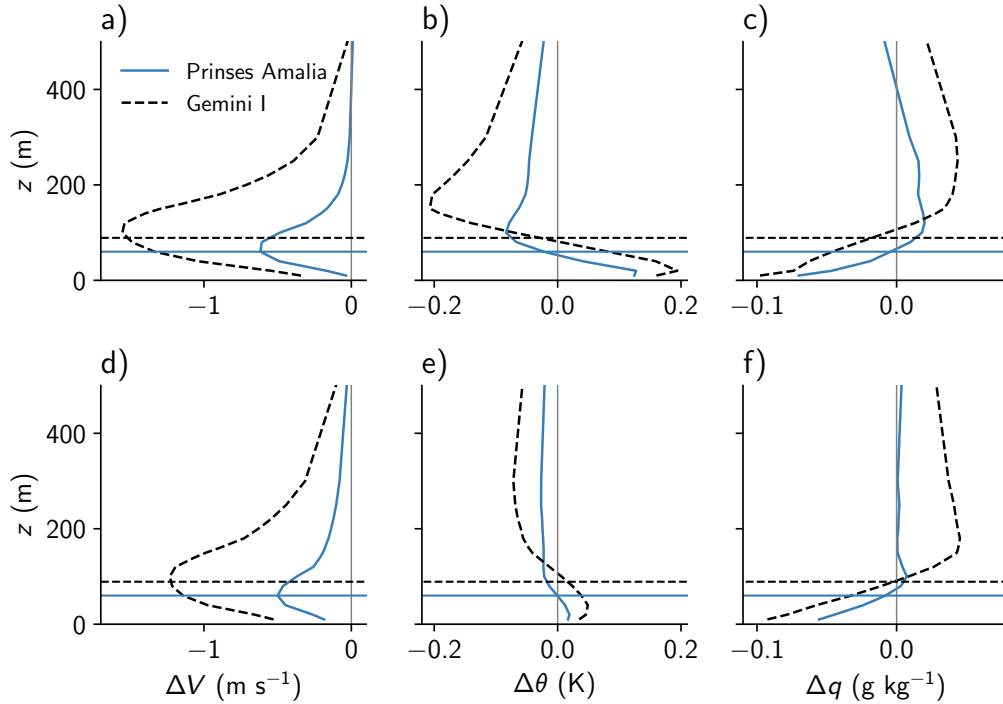


**Figure 10.** Impact of wind turbines on meteorological variables wind velocity (a,d), potential temperature (b,e), and specific humidity (c,f) over two Dutch offshore wind farms, Gemini to the north of the Dutch coast (black dashed) and Prinses Amalia to the west of the Dutch coast (blue solid), where  $\Delta = \text{WFP} - \text{REF}$ . The top panels (a – c) are averaged profiles over 1 March – 30 June 2016, the bottom panels (d – f) are averaged profiles over 1 September – 31 December 2016. The horizontal lines indicate the hub height of each wind farm.

392 MW,  $-1.6 \text{ m s}^{-1}$  during spring and  $-1.2 \text{ m s}^{-1}$  in Autumn). The modelled velocity deficit  
 393 is shown to be stronger in the spring season with relatively more stable cases. Previous  
 394 research has also shown higher velocity deficits during stable cases compared to unsta-  
 395 ble atmospheric boundary layers (e.g. Dörenkämper et al., 2015).

396 The enhanced vertical mixing has a weak impact on temperature and specific hu-  
 397 midity. During the period where the atmosphere is on average stably stratified, the en-  
 398 hanced TKE and vertical mixing decreases the stratification, resulting in an increase in  
 399 temperature and decrease in specific humidity near the surface, and decrease in temper-  
 400 ature and increase in specific humidity at 100-150 m height. At the large wind farm, Gem-  
 401 ini, this average vertical potential temperature variation is between  $-0.2$  and  $0.2 \text{ K}$ , for  
 402 the smaller wind farm (Prinses Amalia)  $-0.08$  to  $0.12 \text{ K}$ . The specific humidity during  
 403 spring, decreases  $-0.1$  for Gemini and  $-0.07 \text{ g kg}^{-1}$  for Prinses Amalia near the surface

404 and increases by 0.04 and 0.02 g kg<sup>-1</sup>, respectively, above hub height. As a result of the  
405 near surface heating and drying, and the cooling and moistening aloft, the relative hu-  
406 midity decreases near the surface, and increases higher up. This could impact the for-  
407 mation of fog or low clouds.

408 During autumn and early winter the influence of the enhanced vertical mixing by  
409 wind turbines is smaller, for potential temperature less than 0.1 K for both wind farms.  
410 The well-mixed profiles during unstable conditions are barely influenced by enhanced TKE.  
411 However, the near-surface moisture is reduced by the same order of magnitude in the au-  
412 tumn compared to the spring season.

## 413 **7 Conclusion**

414 The Fitch et al. (2012) wind-farm parameterisation was implemented in mesoscale  
415 model HARMONIE-AROME, and validated with a variety of observations in the north-  
416 sea region over a one-year period. The parameterisation reduces momentum and con-  
417 verts this into turbulent kinetic energy and power production, depending on wind tur-  
418 bine properties. Two year-long simulations were performed, one including all wind tur-  
419 bines on the North Sea known up to 2016 and one without any wind turbines. The eval-  
420 uation with various wind measurements on the North Sea indicates that inclusion of the  
421 turbine parameterisation has a positive impact on the modelled wind speeds near (off-  
422 shore) wind farms. For all locations considered, the absolute bias in wind speed is de-  
423 creased compared to the simulation without wind farms. Furthermore, the predicted power  
424 production – compared to observations from the Belgian TSO – shows a substantial im-  
425 provement with the turbine parameterisation included.

426 A brief survey of the impact of wind farms on the local meteorological conditions,  
427 indicates that in addition to changes in wind speed, other quantities like temperature  
428 or humidity are influenced by wind farms as well. These variations in temperature and  
429 humidity are more pronounced in periods with more stable conditions, where the enhanced  
430 turbulent kinetic energy from the wind turbines increases the mixing of the marine bound-  
431 ary layer. With the expected increase in number and size of wind turbines in the com-  
432 ing decades the influence of wind turbines on local to regional meteorology can no longer  
433 be neglected. The relatively simple wind-farm parameterisation by Fitch et al. (2012)

434 improves modelled wind speed near wind farms and can be used operationally to improve  
435 weather forecasts and predicted power production.

### 436 **Acknowledgments**

437 The authors would like to acknowledge funding from the Dutch Offshore Wind Atlas (DOWA)  
438 project supported with Topsector Energy subsidy from the Ministry of Economic Affairs  
439 and Climate Policy, and the Topconsortia for Knowledge and Innovation (TKI) funded  
440 Winds of the North Sea in 2050 (WINS50) project. The authors would like to thank ECMWF  
441 for providing computational resources. We would also like to thank Jeanette Onvlee, Sukanta  
442 Basu, and Pier Siebesma for fruitful discussions.

### 443 **Data availability**

444 The HARMONIE-AROME model simulations are available on the KNMI data platform:  
445 <https://dataplatform.knmi.nl/dataset/?tags=Dutch+Offshore+Wind+Atlas>

### 446 **Appendix A Wind farm and turbine information**

447 Tables A1 and A2 provide an overview of all the wind farms implemented in the  
448 experimental domain, and Table A3 summarises the turbine types and their properties.

### 449 **References**

- 450 Abkar, M., & Porté-Agel, F. (2015). A new wind-farm parameterization for large-  
451 scale atmospheric models. *Journal of Renewable and Sustainable Energy*, 7(1),  
452 013121.
- 453 Acker, T., & Chime, A. H. (2011). Wind modeling using windpro and wasp software.  
454 *Norther Arizon University, USA, 1560000(8.8)*, 510.
- 455 Baidya Roy, S., & Traiteur, J. J. (2010). Impacts of wind farms on surface air tem-  
456 peratures. *Proceedings of the National Academy of Sciences*, 107(42), 17899–  
457 17904.
- 458 Banta, R. M., Pichugina, Y. L., Brewer, W. A., Lundquist, J. K., Kelley, N. D.,  
459 Sandberg, S. P., ... Weickmann, A. M. (2015). 3d volumetric analysis of wind  
460 turbine wake properties in the atmosphere using high-resolution doppler lidar.  
461 *Journal of Atmospheric and Oceanic Technology*, 32(5), 904–914.

| Name                 | Latitude (°N) | Longitude (°E) | Turbine type | N   | Z (m) |
|----------------------|---------------|----------------|--------------|-----|-------|
| London Array 1       | 51.626        | 1.496          | SWT-3.6-120  | 175 | 87    |
| Gemini               | 54.036        | 5.963          | SWT-4.0-130  | 150 | 89    |
| Gode Wind I          | 54.016        | 6.983          | SWT-6.0-154  | 55  | 110   |
| Gode Wind II         | 54.075        | 7.007          | SWT-6.0-154  | 42  | 110   |
| Gwynt y Mor          | 53.460        | -3.599         | SWT-3.6-107  | 160 | 98    |
| Race Bank            | 53.276        | 0.841          | SWT-6.0-154  | 91  | 110   |
| Greater Gabbard      | 51.773        | 1.982          | SWT-3.6-107  | 140 | 78    |
| Dudgeon              | 53.265        | 1.380          | SWT-6.0-154  | 67  | 110   |
| Veja Mate            | 54.321        | 5.860          | SWT-6.0-154  | 67  | 103   |
| Anholt               | 56.600        | 11.210         | SWT-3.6-120  | 111 | 82    |
| Bard Offshore 1      | 54.355        | 5.980          | BARD-5.0     | 80  | 90    |
| GlobalTech I         | 54.500        | 6.358          | Areva-5.0    | 80  | 90    |
| Rampion Wind Farm    | 50.660        | -0.200         | V112-3.45    | 116 | 84    |
| West of Duddon Sands | 53.984        | -3.464         | SWT-3.6-120  | 108 | 80    |
| Walney 1             | 53.810        | -4.907         | SWT-3.6-107  | 51  | 84    |
| Walney 2             | 54.081        | -3.605         | SWT-3.6-107  | 51  | 90    |
| Galloper             | 51.880        | 2.040          | SWT-6.0-154  | 56  | 103   |
| Wikinger Offshore    | 54.834        | 14.068         | Adwen-5.0    | 70  | 75    |
| Nordsee One Offshore | 54.444        | 7.682          | Senvion-6.2  | 54  | 100   |
| Sheringham Shoal     | 53.135        | 1.147          | SWT-3.6-107  | 88  | 82    |
| Borkum Riffgrund I   | 53.967        | 6.562          | SWT-4.0-12   | 78  | 87    |
| Borkum Riffgrund II  | 53.967        | 6.496          | V164-8.0     | 56  | 105   |
| Amrumbank West       | 54.520        | 7.708          | SWT-3.6-120  | 80  | 90    |
| Thanet               | 51.430        | 1.633          | V90-3.0      | 100 | 70    |
| Nordsee Ost          | 54.444        | 7.682          | Senvion-6.2  | 48  | 97    |
| Butendiek            | 55.019        | 7.774          | SWT-3.6-120  | 80  | 91    |
| Dan Tysk             | 55.140        | 7.200          | SWT-3.6-120  | 80  | 88    |
| Baltica 2            | 55.070        | 17.100         | SWT-3.6-120  | 80  | 78    |
| Meerwind Sued/Ost    | 54.402        | 7.707          | SWT-3.6-120  | 80  | 89    |
| Sandbank             | 55.190        | 6.860          | SWT-4.0-130  | 72  | 95    |
| Lincs                | 53.191        | 0.491          | SWT-3.6-120  | 75  | 100   |
| Burbo Bank Extension | 53.483        | -3.273         | V164-8.0     | 32  | 123   |
| Humber Gateway       | 53.619        | 0.293          | V112-3.0     | 73  | 80    |

**Table A1.** Overview of wind farms included in the experiments. Latitude and longitude indicate the location in the centre of the wind farm. N are the number of turbines in the wind farm and Z is the hub height.

| Name                   | Latitude (°N) | Longitude (°E) | Turbine type | N  | Z (m) |
|------------------------|---------------|----------------|--------------|----|-------|
| Westermost Rough       | 53.805        | 0.149          | SWT-6.0-154  | 35 | 100   |
| Horns Rev 2            | 55.600        | 7.582          | SWT-2.3-93   | 91 | 68    |
| Rodsand II             | 54.558        | 11.531         | SWT-2.3-93   | 90 | 69    |
| Trianel Borkum II      | 54.042        | 6.467          | Areva-5.0    | 40 | 90    |
| Kentish Flats 1        | 51.460        | 1.093          | V90-3.0      | 30 | 70    |
| Kentish Flats 2        | 51.450        | 1.079          | V112-3.3     | 15 | 84    |
| Gunfleet Sands         | 51.737        | 1.170          | SWT-3.6-107  | 48 | 75    |
| Ormonde                | 54.088        | -3.437         | Senvion-5    | 30 | 97    |
| Barrow                 | 53.982        | -3.283         | V90-3.0      | 30 | 75    |
| Rhyl Flats             | 53.380        | -3.646         | SWT-3.6-107  | 25 | 75    |
| North Hoyle            | 53.417        | -3.448         | V80-2.0      | 30 | 67    |
| Riffgat                | 53.692        | 6.470          | SWT-3.6-120  | 30 | 90    |
| Horns Rev 1            | 55.486        | 7.840          | V80-2.0      | 80 | 70    |
| Nysted                 | 54.549        | 11.714         | SWT-2.3-82   | 72 | 69    |
| EnBW Baltic 1          | 54.596        | 12.638         | SWT-2.3-93   | 21 | 67    |
| EOWDC                  | 57.230        | -1.990         | V164-8.0     | 11 | 120   |
| Hywind 2 Demonstration | 57.500        | -1.300         | SWT-6.0-154  | 5  | 98    |
| Arkonabecken Südost    | 54.780        | 14.120         | SWT-6.0-154  | 60 | 102   |
| Alpha Ventus           | 54.017        | 6.600          | Avera-5.0    | 12 | 90    |
| Walney Extension 3     | 54.087        | -3.737         | V164-8.0     | 40 | 113   |
| Walney Extension 4     | 54.087        | -3.737         | SWT-7.0-154  | 47 | 111   |
| Luchterduinen          | 52.403        | 4.165          | V112-3.0     | 43 | 81    |
| Prinses Amalia         | 52.594        | 4.213          | V80-2.0      | 60 | 59    |
| Egmond aan Zee         | 52.594        | 4.437          | V90-3.0      | 36 | 70    |
| Belwind I              | 51.670        | 2.800          | V90-3.0      | 55 | 72    |
| Northwind              | 51.619        | 2.901          | V112-3.0     | 72 | 71    |
| Thorntonbank           | 51.540        | 2.940          | Multiple     | 54 | 95    |

**Table A2.** Table A1 continued

| Name                | N   | P (MW) | D (m) |     |
|---------------------|-----|--------|-------|-----|
| Siemens SWT-2.3-82  | 72  | 2.3    | 72    |     |
| Siemens SWT-2.3-93  | 202 | 2.3    | 93    |     |
| Siemens SWT-3.6-107 | 563 | 3.6    | 107   |     |
| Siemens SWT-3.6-120 | 899 | 3.6    | 120   |     |
| Siemens SWT-4.0-120 | 78  | 4.0    | 120   |     |
| Siemens SWT-4.0-130 | 222 | 4.0    | 130   |     |
| Siemens SWT-6.0-154 | 478 | 6.0    | 154   | (1) |
| Siemens SWT-7.0-154 | 47  | 7.0    | 154   | (1) |
| Vestas V80-2.0      | 170 | 2.0    | 80    |     |
| Vestas V90-3.0      | 251 | 3.0    | 90    |     |
| Vestas V112-3.0     | 188 | 3.0    | 112   |     |
| Vestas V112-3.3     | 15  | 3.3    | 112   |     |
| Vestas V112-3.45    | 116 | 3.45   | 112   |     |
| Vestas V164-8.0     | 139 | 8.0    | 164   | (2) |
| Senvion 5           | 30  | 5.0    | 126   |     |
| Senvion 6.2         | 156 | 6.2    | 126   |     |
| BARD-5.0            | 80  | 5.0    | 126   | (3) |
| Adwen-5.0           | 202 | 5.0    | 116   | (3) |
| Haliade-6           | 1   | 6.0    | 100   |     |

3908  $460 \times 10^3$

**Table A3.** Overview of the wind turbine types included in the experiments. The total installed power equals  $\sum N \times P$ . Notes: (1) replaced with 6 MW reference turbine from (Bulder et al., 2016), (2) replaced with 8 MW reference turbine from (Bulder et al., 2016), (3) replaced with Senvion 5 turbine.

- 462 Bärffuss, K., Hankers, R., Bitter, M., Feuerle, T., Schulz, H., Rausch, T., ... Lam-  
463 pert, A. (2019). In-situ airborne measurements of atmospheric and sea surface  
464 parameters related to offshore wind parks in the german bight. *PANGAEA*  
465 <https://doi.org/10.1594/PANGAEA.902845>.
- 466 Bengtsson, L., Andrae, U., Aspelien, T., Batrak, Y., Calvo, J., de Rooy, W., ... oth-  
467 ers (2017). The HARMONIE-AROME model configuration in the ALADIN-  
468 HIRLAM NWP system. *Monthly Weather Review*, 145(5), 1919–1935.
- 469 Bulder, B., Bot, E., & Marina, A. (2016). *Scoping analysis of the potential yield*  
470 *of the Hollandse Kust (zuid) wind farm sites and the influence on the existing*  
471 *wind farms in the proximity* (Tech. Rep. No. ECN-E-16-021 - 2nd edt.) ECN.
- 472 Christiansen, M. B., & Hasager, C. B. (2005). Wake effects of large offshore wind  
473 farms identified from satellite sar. *Remote Sensing of Environment*, 98(2-3),  
474 251–268.
- 475 de Haan, S. (2011). High-resolution wind and temperature observations from aircraft  
476 tracked by Mode-S air traffic control radar. *Journal of Geophysical Research:*

- 477 *Atmospheres*, 116(D10).
- 478 de Haan, S. (2016). Estimates of Mode-S EHS aircraft-derived wind observation  
 479 errors using triple collocation. *Atmospheric Measurement Techniques*, 9(8),  
 480 4141–4150.
- 481 de Rooy, W. C., Siebesma, P., Baas, P., Lenderink, G., de Roode, S., de Vries, H.,  
 482 ... van 't Veen, B. (2021). Model development in practice: A comprehensive  
 483 update to the boundary layer schemes in HARMONIE-AROME. *Geoscientific*  
 484 *Model Development*, -( ), -.
- 485 Dörenkämper, M., Witha, B., Steinfeld, G., Heinemann, D., & Kühn, M. (2015).  
 486 The impact of stable atmospheric boundary layers on wind-turbine wakes  
 487 within offshore wind farms. *Journal of Wind Engineering and Industrial Aero-*  
 488 *dynamics*, 144, 146–153.
- 489 Duncan, J. B., Wijnant, I. L., & Knoop, S. (2019). *DOWA validation against off-*  
 490 *shore mast and LiDAR measurements*. (Tech. Rep. No. TNO Technical Report  
 491 2019 R10062). Retrieved from [https://www.dutchoffshorewindatlas.nl/](https://www.dutchoffshorewindatlas.nl/publications/reports/2019/05/21/tno-report-dowa-validation-against-offshore-mast-and-lidar-measurements)  
 492 [publications/reports/2019/05/21/tno-report-dowa-validation-against](https://www.dutchoffshorewindatlas.nl/publications/reports/2019/05/21/tno-report-dowa-validation-against-offshore-mast-and-lidar-measurements)  
 493 [-offshore-mast-and-lidar-measurements](https://www.dutchoffshorewindatlas.nl/publications/reports/2019/05/21/tno-report-dowa-validation-against-offshore-mast-and-lidar-measurements)
- 494 Faroux, S., Kaptué Tchuenté, A., Roujean, J.-L., Masson, V., Martin, E., & Moigne,  
 495 P. L. (2013). Ecoclimap-ii/europe: A twofold database of ecosystems and  
 496 surface parameters at 1 km resolution based on satellite information for use in  
 497 land surface, meteorological and climate models. *Geoscientific Model Develop-*  
 498 *ment*, 6(2), 563–582.
- 499 Fischer, C., Montmerle, T., Berre, L., Auger, L., & Ştefănescu, S. E. (2005). An  
 500 overview of the variational assimilation in the ALADIN/France numerical  
 501 weather-prediction system. *Quarterly Journal of the Royal Meteorological*  
 502 *Society*, 131(613), 3477–3492.
- 503 Fischereit, J., Brown, R., Larsén, X. G., Badger, J., & Hawkes, G. (2021). Review of  
 504 mesoscale wind-farm parametrizations and their applications. *Boundary-Layer*  
 505 *Meteorology*, 1–50.
- 506 Fitch, A. C., Olson, J. B., Lundquist, J. K., Dudhia, J., Gupta, A. K., Michalakes,  
 507 J., & Barstad, I. (2012). Local and mesoscale impacts of wind farms as pa-  
 508 rameterized in a mesoscale NWP model. *Monthly Weather Review*, 140(9),  
 509 3017–3038.

- 510 Gustafsson, N., Janjić, T., Schraff, C., Leuenberger, D., Weissmann, M., Reich, H.,  
 511 ... others (2018). Survey of data assimilation methods for convective-scale  
 512 numerical weather prediction at operational centres. *Quarterly Journal of the*  
 513 *Royal Meteorological Society*, *144*(713), 1218–1256.
- 514 Hersbach, H., Bell, B., Berrisford, P., Hirahara, S., Horányi, A., Muñoz-Sabater, J.,  
 515 ... others (2020). The era5 global reanalysis. *Quarterly Journal of the Royal*  
 516 *Meteorological Society*, *146*(730), 1999–2049.
- 517 Lampert, A., Bärffuss, K., Platis, A., Siedersleben, S., Djath, B., Cañadillas, B., ...  
 518 others (2020). In situ airborne measurements of atmospheric and sea surface  
 519 parameters related to offshore wind parks in the german bight. *Earth System*  
 520 *Science Data*, *12*(2), 935–946.
- 521 Lampert, A., Bärffuss, K., Platis, A., Siedersleben, S., Djath, B., Cañadillas,  
 522 B., ... Emeis, S. (2020). In situ airborne measurements of atmo-  
 523 spheric and sea surface parameters related to offshore wind parks in the  
 524 german bight. *Earth System Science Data*, *12*(2), 935–946. Retrieved  
 525 from <https://essd.copernicus.org/articles/12/935/2020/> doi:  
 526 10.5194/essd-12-935-2020
- 527 Lee, J. C., & Lundquist, J. K. (2017). Evaluation of the wind farm parameterization  
 528 in the weather research and forecasting model (version 3.8. 1) with meteorolo-  
 529 gical and turbine power data. *Geoscientific Model Development*, *10*(11),  
 530 4229–4244.
- 531 Lenderink, G., & Holtslag, A. A. (2004). An updated length-scale formulation for  
 532 turbulent mixing in clear and cloudy boundary layers. *Quarterly Journal of the*  
 533 *Royal Meteorological Society: A journal of the atmospheric sciences, applied*  
 534 *meteorology and physical oceanography*, *130*(604), 3405–3427.
- 535 Marseille, G.-J., & Stoffelen, A. (2017). Toward scatterometer winds assimilation  
 536 in the mesoscale harmonie model. *IEEE Journal of Selected Topics in Applied*  
 537 *Earth Observations and Remote Sensing*, *10*(5), 2383–2393.
- 538 Martín Míguez, B., Novellino, A., Vinci, M., Claus, S., Calewaert, J.-B., Vallius, H.,  
 539 ... others (2019). The european marine observation and data network (emod-  
 540 net): visions and roles of the gateway to marine data in europe. *Frontiers in*  
 541 *Marine Science*, *6*, 313.
- 542 Masson, V., Le Moigne, P., Martin, E., Faroux, S., Alias, A., Alkama, R., ... oth-

- 543 ers (2013). The surfexv7. 2 land and ocean surface platform for coupled or  
 544 offline simulation of earth surface variables and fluxes. *Geoscientific Model*  
 545 *Development*, 6(4), 929–960.
- 546 Muñoz-Esparza, D., Cañadillas, B., Neumann, T., & Van Beeck, J. (2012). Turbu-  
 547 lent fluxes, stability and shear in the offshore environment: Mesoscale mod-  
 548 elling and field observations at fino1. *Journal of Renewable and Sustainable*  
 549 *Energy*, 4(6), 063136.
- 550 Platis, A., Bange, J., Bärffuss, K., Cañadillas, B., Hundhausen, M., Djath, B., ...  
 551 others (2020). Long-range modifications of the wind field by offshore wind  
 552 parks—results of the project wipaff. *Meteorologische Zeitschrift*, 355–376.
- 553 Platis, A., Hundhausen, M., Mauz, M., Siedersleben, S., Lampert, A., Bärffuss, K.,  
 554 ... others (2021). Evaluation of a simple analytical model for offshore wind  
 555 farm wake recovery by in situ data and weather research and forecasting simu-  
 556 lations. *Wind Energy*, 24(3), 212–228.
- 557 Rhodes, M. E., & Lundquist, J. K. (2013). The effect of wind-turbine wakes on sum-  
 558 mertime us midwest atmospheric wind profiles as observed with ground-based  
 559 doppler lidar. *Boundary-layer meteorology*, 149(1), 85–103.
- 560 Shepherd, T., Barthelmie, R., & Pryor, S. (2020). Sensitivity of wind turbine ar-  
 561 ray downstream effects to the parameterization used in wrf. *Journal of Applied*  
 562 *Meteorology and Climatology*, 59(3), 333–361.
- 563 Skamarock, W. C., Klemp, J. B., Dudhia, J., Gill, D. O., Liu, Z., Berner, J., ...  
 564 others (2019). A description of the advanced research wrf model version 4.  
 565 *National Center for Atmospheric Research: Boulder, CO, USA*, 145.
- 566 Volker, P., Badger, J., Hahmann, A. N., & Ott, S. (2015). The explicit wake  
 567 parametrisation v1. 0: a wind farm parametrisation in the mesoscale model  
 568 wrf. *Geoscientific Model Development*, 8(11), 3715–3731.
- 569 Wagner, D., Steinfeld, G., Witha, B., Wurps, H., & Reuder, J. (2019). Low level jets  
 570 over the southern north sea. *Meteorologische Zeitschrift*, 389–415.
- 571 Westerhellweg, A., Canadillas, B., Beeken, A., & Neumann, T. (2010). One year  
 572 of lidar measurements at fino1-platform: Comparison and verification to met-  
 573 mast data. In *Proceedings of 10th german wind energy conference dewek* (pp.  
 574 1–5).
- 575 Westerhellweg, A., Neumann, T., & Riedel, V. (2012). Fino1 mast correction.

576 *DEWI-Magazin*, 21.

577 Wijnant, I. L., van Ulf, B., van Stratum, B. J. H., Barkmeijer, J., Onvlee, J., de  
578 Valk, S., C. Knoop, ... Klein Baltink, H. (2019). *The dutch offshore wind*  
579 *atlas (DOWA): description of the dataset* (Tech. Rep.). Retrieved from  
580 <https://www.dutchoffshorewindatlas.nl/publications>

581 WindEurope. (2017). *Wind energy in europe: Scenarios for 2030* (Tech. Rep.).  
582 Retrieved from [https://windeurope.org/wp-content/uploads/files/](https://windeurope.org/wp-content/uploads/files/about-wind/reports/Wind-energy-in-Europe-Scenarios-for-2030.pdf)  
583 [about-wind/reports/Wind-energy-in-Europe-Scenarios-for-2030.pdf](https://windeurope.org/wp-content/uploads/files/about-wind/reports/Wind-energy-in-Europe-Scenarios-for-2030.pdf)

584 Witkin, A. P., & Heckbert, P. S. (2005). Using particles to sample and control im-  
585 plicit surfaces. In *Acm siggraph 2005 courses* (p. 260).

586 Wu, C., Luo, K., Wang, Q., & Fan, J. (2022). A refined wind farm parameterization  
587 for the weather research and forecasting model. *Applied Energy*, 306, 118082.

588 Zhan, L., Letizia, S., & Valerio Iungo, G. (2020). Lidar measurements for an on-  
589 shore wind farm: Wake variability for different incoming wind speeds and  
590 atmospheric stability regimes. *Wind Energy*, 23(3), 501–527.